

Single-Molecule Conductance of Viologen–Cucurbit[8]uril Host–Guest Complexes

Wei Zhang,^{†,‡,§} Shiyu Gan,[†] Andrea Vezzoli,[§] Ross J. Davidson,^{||} David C. Milan,[§] Konstantin V. Luzyanin,[§] Simon J. Higgins,[§] Richard J. Nichols,^{*,§} Andrew Beeby,^{||} Paul J. Low,[⊥] Buyi Li,[§] and Li Niu^{*,†}

[†]State Key Laboratory of Electroanalytical Chemistry, CAS Center for Excellence in Nanoscience, c/o Engineering Laboratory for Modern Analytical Techniques, Changchun Institute of Applied Chemistry, Chinese Academy of Sciences, Changchun 130022, China

[‡]University of Chinese Academy of Sciences, Beijing 100049, China

[§]Department of Chemistry, University of Liverpool, Crown Street, Liverpool L69 7ZD, United Kingdom

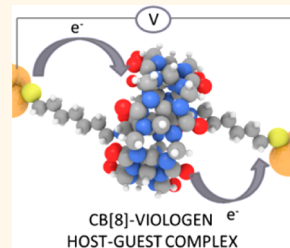
^{||}Department of Chemistry, Durham University, South Road, Durham DH1 3LE, United Kingdom

[⊥]School of Chemistry and Biochemistry, University of Western Australia, 35 Stirling Highway, Perth, Western Australia 6009, Australia

Supporting Information

ABSTRACT: The local molecular environment is a critical factor which should be taken into account when measuring single-molecule electrical properties in condensed media or in the design of future molecular electronic or single molecule sensing devices. Supramolecular interactions can be used to control the local environment in molecular assemblies and have been used to create microenvironments, for instance, for chemical reactions. Here, we use supramolecular interactions to create microenvironments which influence the electrical conductance of single molecule wires. Cucurbit[8]uril (CB[8]) with a large hydrophobic cavity was used to host the viologen (bipyridinium) molecular wires forming a 1:1 supramolecular complex. Significant increases in the viologen wire single molecule conductances are observed when it is threaded into CB[8] due to large changes of the molecular microenvironment. The results were interpreted within the framework of a Marcus-type model for electron transfer as arising from a reduction in outer-sphere reorganization energy when the viologen is confined within the hydrophobic CB[8] cavity.

KEYWORDS: STM, single molecule conductance, cucurbituril, viologen, host–guest complexes



The ability to measure the electrical properties of single molecules bridging between two metal contacts, based on the use of mechanically controlled break junctions (MCBJ)^{1–3} or scanning probes techniques such as STM^{4–6} or conducting AFM,⁷ has given a great boost to the field of molecular electronics over the last 15 years.⁸ Charge-transport mechanisms, long-range low-attenuation factor molecular wires,^{9–13} conductance switching, and single molecule transistor effects^{14,15} have been subjects of ongoing interest in the literature. As knowledge of these mechanisms grows, molecules of increasing chemical complexity have become more amenable to study. Attention has therefore been directed toward not only single molecules but also supramolecular assemblies.¹⁶ Examples of supramolecular interactions being exploited in molecular junctions include π -stacking between pairs of oligo(phenylene ethynylene) (OPE) molecular wires,^{17,18} hydrogen bonding between facing pairs of carboxylic acids,¹⁹ noncovalently linked porphyrin–fullerene dyads,²⁰ molecular donor–acceptor complexation,^{21,22} hydrogen bonding of

nucleotides,²³ and rotaxane-based memory cells.¹⁶ Supramolecular interactions have been previously used to inhibit aggregation of molecular wires in junctions and thereby promote the formation of single molecular junctions for molecules.²⁴ Kiguchi *et al.* reported the formation of molecular junctions assembled from a single π -conjugated molecular wire threaded within α -cyclodextrin.²⁴ This study found that such encapsulation leads to reduced conductance and a reduced spread of conductance values; the latter was attributed to damping of intramolecular conformational mobility of the molecular wire as well as the elimination of intermolecular interactions.²⁴

Our group has previously studied the influence of water on the single molecule conductance.²⁵ In this present study we take a different approach to control the microenvironment of

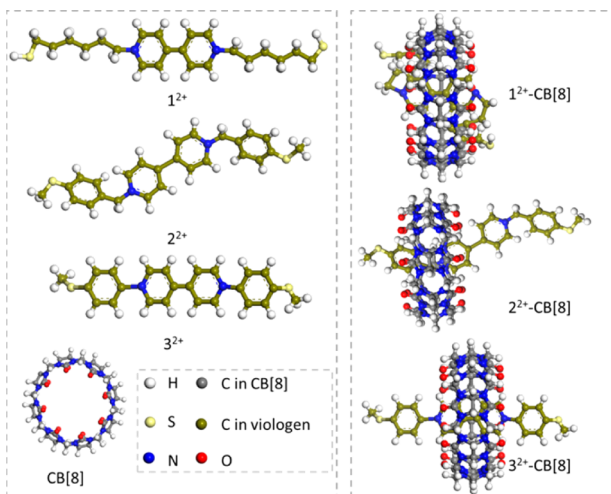
Received: January 31, 2016

Accepted: April 7, 2016

Published: April 7, 2016

single molecule wires by employing host–guest supramolecular interactions between cucurbit[8]uril (CB[8]) and viologen molecular bridges.⁵ CB[8] is a macrocycle with eight glycol-uril units and has been described as having a pumpkin²⁶ or barrel shape (see Scheme 1 and the Supporting Information (SI),

Scheme 1. Structures of Viologens and CB[8]^{4a}



^a1²⁺, 2²⁺, 3²⁺ (left, from top to down) and 1²⁺–CB[8], 2²⁺–CB[8], 3²⁺–CB[8] (right, from top to down) are shown as their thiol or thioether form, and counterions are omitted.

Figure S8). CB[8] macrocycles have identical carbonyl lined rims at either end. These are highly polar especially when compared to the main cavity, which is considered to be hydrophobic.^{26–33} Host–guest complexes of CB[8] and viologen derivatives have been studied in detail,^{26–28,34–39} with the strong dipole–dipole and hydrophobic interactions between these components resulting in binding constants of up to 10⁶.²⁸ Recently, a method has been presented for the assembly of surface-immobilized viologens threaded by CB[8],³³ which has provided inspiration for our present investigations of CB[8]:viologen assemblies within single molecular electrical junctions.

In the present work, we explore the single molecule conductance of three different viologen-based molecular wires, 6-[1'-(6-mercaptohexyl)[4,4']bipyridinium]hexane-1-thiol bromide (1²⁺), 1,1'-bis(4-(methylthio)benzyl)[4,4'-bipyridine]-1,1'-dium bromide (2²⁺), and 1,1'-bis(4-(methylthio)phenyl)-[4,4'-bipyridine]-1,1'-dium chloride (3²⁺) (Scheme 1), and their supramolecular assemblies when threaded through CB[8]. The well-known bis(hexylthiol) compound 1²⁺^{5,40,41} is prepared and stored as the thioacetyl-protected derivative.⁴⁰ The thioacetyl groups are readily liberated on exposure to gold surfaces resulting in binding of the compounds via strong gold–sulfur interactions. The benzyl derivative 2²⁺ and phenyl derivative 3²⁺ feature the thioether –SMe functional group as a surface-contacting moiety.⁴² The –SMe group has attracted attention in recent years as an alternative to the thiolate/thioacetyl moiety.⁴² While the Au–S(Me) contact has been found to be less electrically transparent than Au–S in studies carried out to date, resulting in slightly lower conductance values, it is more readily introduced into a range of complex molecular structures, does not require removal of the protecting group, and offers a contact “strength” (Au–S(Me) bond rupture force) which is comparable to those of other well-

known contacting groups such as –NH₂ and pyridine.⁴³ We show here that encapsulation of these viologen wires in Scheme 1 by CB[8] is seen to markedly impact their single-molecule conductance, and possible mechanisms of this conductance gating are discussed. Since host:guest assembly between the three viologen molecular targets has not been examined before, a detailed characterization is also included, with the host–guest complexation being examined by ¹H NMR spectroscopy, mass spectrometry, ultraviolet–visible (UV/vis) spectroscopy, and cyclic voltammetry (CV).

RESULTS

Spectroscopic Characterization for Viologen–CB[8] Interaction. It has been reported that a variety of alkyl viologen derivatives form host–guest complexes with CB[8] with inclusion constants (*K*) up to ~10⁶.²⁸ However, the binding between 1²⁺, 2²⁺, and 3²⁺ and CB[8], respectively, has not been previously investigated. To clarify the binding stoichiometry of these three viologen compounds with CB[8] we have recorded mass spectra. Mass spectra (ESI⁺) of 1²⁺–CB[8], 2²⁺–CB[8], and 3²⁺–CB[8] are shown in Figures S9–S14. The *m/z* value for 1²⁺–CB[8] is 859.3, and this is consistent with a 1:1 complex of the viologen dication. For 2²⁺–CB[8], mass spectrometry data show the base peak at *m/z* = 879.8 amu, while 3²⁺–CB[8] gives a base peak at *m/z* = 865.3 amu. In each case, the isotope pattern shows a 0.5 amu progression, consistent with the dicationic nature of these assemblies, with a mass/charge ratio consistent with the formation of the 1:1 viologen/CB[8] complex.

The HRMS (ESI⁺, Q-TOF) data for 1²⁺–CB[8] and 3²⁺–CB[8] further demonstrate the formation of a 1:1 complex between 1²⁺ or 3²⁺ and CB[8]. For 2²⁺, its CB[8] complex HRMS (ESI⁺, Q-TOF) data demonstrated that the 1:1 complex 2²⁺–CB[8] is the predominant form, although a low intensity ion peak at higher mass (*m/z* 1544) corresponding to the binding of two molecules of CB[8] by the viologen dication was also observed (Figure S13). Given the nature of the binding site of the CB[8] moiety along the molecular “thread” of 2²⁺ (Scheme 1 and discussion below), such 1:2 viologen/CB[8] assemblies are not unexpected.

UV/vis spectra of 1²⁺(Br[−])₂, 2²⁺(Br[−])₂, and 3²⁺(Cl[−])₂ in the absence and presence of CB[8] were recorded. Solutions of 1²⁺(Br[−])₂ are colorless (*i.e.*, do not absorb between 300–800 nm) but rather contain an absorption band in the UV region centered at 261 nm. With the addition of CB[8] there is a small red shift of the absorption band from 261 to 263 nm and a decrease in molar absorptivity (Figure 1b). This decrease in absorptivity of the peak around 260 nm of the viologen dication is consistent with reported data for other viologen derivative–CB[8] systems^{34,39} and has been used as evidence for the binding between viologen dications and CB[8] in solution.

UV/vis spectra have also been recorded for 2²⁺ and 3²⁺ in the absence and presence of CB[8]. These spectra are more complex than for 1²⁺ due to the presence of benzyl or phenyl groups appended to the viologen core, which give rise to intramolecular charge transfer and solvatochromism (see the Discussion). We find the notable solution color changes and a red-shifted absorbance band of 2²⁺ and 3²⁺ upon addition of CB[8] (see Figures S15 and S16). Such absorbance band red-shifts of viologen derivative systems induced by CB[8] complexation have been previously noted and attributed to the stabilization LUMO of the viologen core upon formation of the binary CB[8]–acceptor complex.³⁰

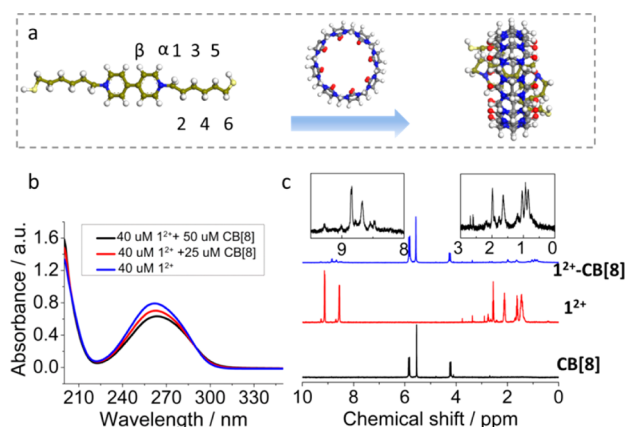


Figure 1. (a) The structure of 1^{2+} with H atom labeling and complexation with CB[8]; (b) UV/vis spectra of 1^{2+} with addition of CB[8]; (c) ^1H NMR spectra of CB[8], 1^{2+} , and 1^{2+} -CB[8]. The inset is for 1^{2+} -CB[8]. The left inset shows a magnification of peaks around 9.0 ppm, while the right inset shows magnification of features around 3.0–0.0 ppm.

^1H NMR spectroscopy was used to investigate the relative position of the dicationic viologen guest within the CB[8] host as well as confirm the host–guest stoichiometry proposed on the basis of the mass spectrometry data. ^1H NMR spectra for all compounds were acquired using solvents suppression via either presaturation or WATERGATE (water suppression by gradient-tailored excitation): see Figure 1c (red line) for the NMR for 1^{2+} , Figure 1c (blue line) for the NMR for 1^{2+} -CB[8], and Figures S17 and S18 for the NMR of 1^{2+} -CB[8] with concentration ratios of 5:1 and 2:1. It should be noted that the peak due to protons 1 of free 1^{2+} indicated in Table S3 (see Figure 1a for numbering scheme) partially overlapped with the solvent signal and were only detected in ^1H NMR experiments without irradiation (not shown in Figure 1c). Upon

incorporation into the host, the protons of the aliphatic carbon chains of 1^{2+} shifted upfield (see Figure 1c, right inset, for a magnified view), while the protons of the CB[8] cage in 1^{2+} -CB[8] exhibit just a slight change compared with the free CB[8]. The upfield shift of the α/α' protons compared to the downfield shift of the β/β' protons upon CB[8] complexation is consistent with these two sets of aromatic protons being in different shielding regions of the CB[8] cavity, with the α/α' protons being shielded and the β/β' ones deshielded. These results indicate that the bipyridinium core is centrally included in the CB[8] host since simple chemical shifts are seen for the bipyridinium core rather than an increased complexity of the splitting pattern. The upfield shift of the aliphatic protons of 1^{2+} upon CB[8] complexation corresponds to them becoming shielded. This increased shielding of these aliphatic protons indicates that they change conformation or environment upon complexation, perhaps either coiling in toward the opening of the host or folding inside the hydrophobic cavity of CB[8] as shown in Figure 1a.³²

The chemical shifts of the 3^{2+} bipyridinium core show similar trends to 1^{2+} upon addition of CB[8] (details can be found in the SI). These results also suggest that the bipyridinium core is included centrally in the CB[8] host. On the other hand, the protons of CB[8] in the complex exhibited large changes when compared with free CB[8], and we also observed the coexistence of the uncomplexed CB[8] in solution together with the 3^{2+} -CB[8] complex. Thus, the 5.83 ppm resonances from free CB[8] appear as two peaks at 5.72 and 5.87 in the complex and starting CB[8], respectively, while the 4.22 ppm resonances split into two peaks at 4.23–4.24 (Figure S19, inset). The ^1H NMR spectra of 2^{2+} -CB[8] are shown in Figure S20, and the $^1\text{H}, ^1\text{H}$ -COSY is in Figure S21. The 2^{2+} -CB[8] complex shows a much more complicated chemical shift pattern than the aforementioned two complexes. This additional complexity for 2^{2+} -CB[8] can be explained by a model

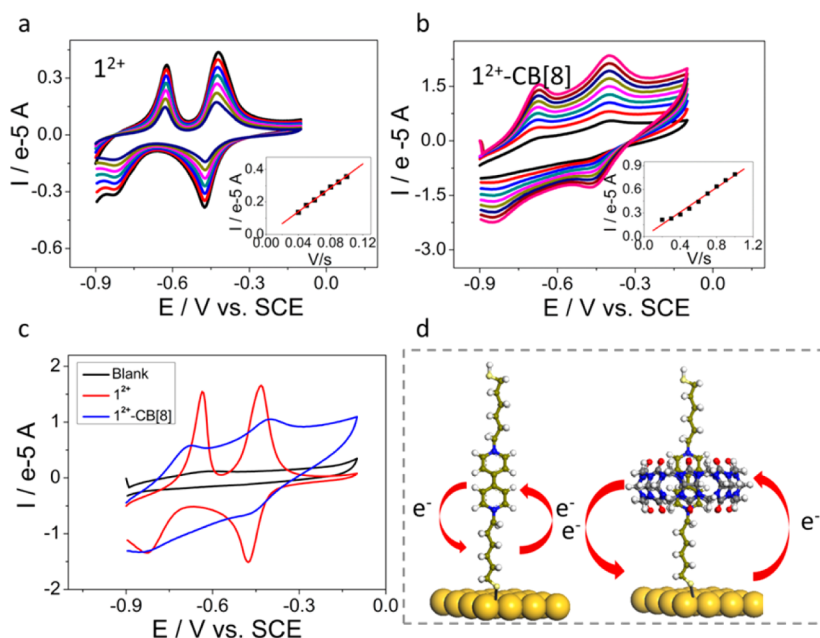


Figure 2. (a) CVs of 1^{2+} monolayer modified Au(111) in 0.1 M PB at different scan rates from 40 to 100 mV/s (inset: corresponding linear relationship between peak height and scan rate); (b) CVs of 1^{2+} -CB[8] monolayer modified Au(111) in 0.1 M PB at different scan rates from 200 to 1000 mV/s (inset: the corresponding linear relationship between peak height and scan rate); (c) CVs of 1^{2+} and 1^{2+} -CB[8] monolayer modified Au(111) in 0.1 M PB at a scan rate of 400 mV/s; (d) scheme of redox reaction for 1^{2+} and 1^{2+} -CB[8].

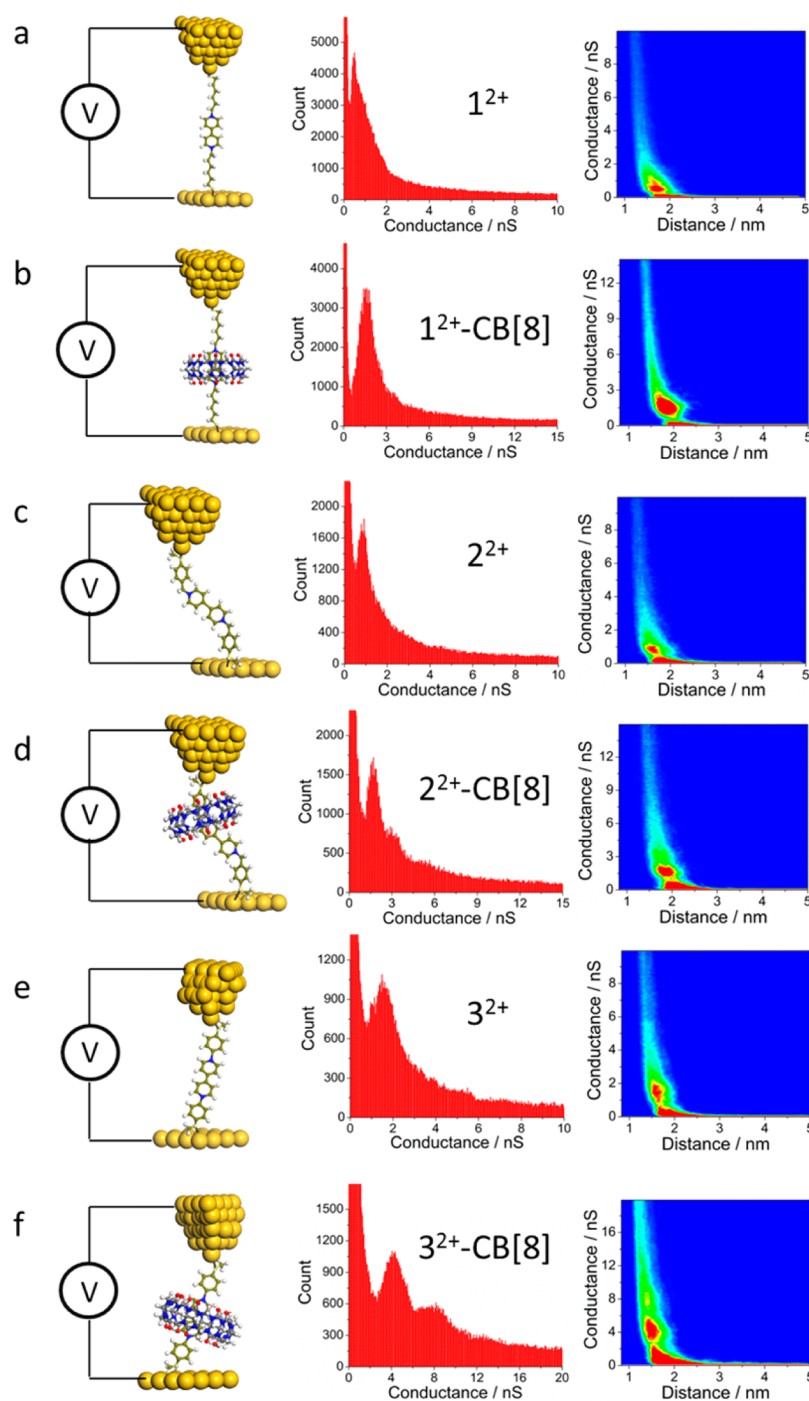


Figure 3. Single molecule conductance measurements: (left column) molecular junction schematic, (center column) 1-D conductance histograms, (right column) 2-D (conductance-junction distance) histograms. The data are for the following junctions 1^{2+} (a), 1^{2+} -CB[8] (b), 2^{2+} (c), 2^{2+} -CB[8] (d), 3^{2+} (e) and 3^{2+} -CB[8] (f).

in which the CB[8] host is positioned asymmetrically with respect to the 2^{2+} guest. In this situation, both phenyl rings exhibit different chemical shifts and give rise to complex patterns. All of the chemical shifts are included in Table S3 (for the 1^{2+} system) and Tables S4 (3^{2+}) and S5 (2^{2+}).

Electrochemical Behavior. The influence of CB[8] on the electrochemical behavior of 1^{2+} monolayers has been investigated both in 0.1 M phosphate buffer (PB, pH 6.98) and 0.1 M NaPF₆ (pH 2.48). Cyclic voltammograms (CVs) of 1^{2+} and 1^{2+} -CB[8] monolayers on Au(111) in PB buffer at different scan rates are shown in Figure 2a,b. CVs recorded in

NaPF₆ are shown in Figures S22 and S23. In PB, two clear redox waves were observed for the 1^{2+} monolayer. The $-0.42/-0.47$ V pair of redox peaks are assigned to the process $1^{2+} \leftrightarrow 1^{*+}$, while the $-0.63/-0.83$ V redox peaks correspond to $1^{*+} \leftrightarrow 1^0$. These values show that there is a significant variation in $E_p^a - E_p^c$ values (the potential difference between the anodic and cathodic waves) for each wave. This and differences in $E_p^a - E_p^c$ values for CVs of the first reduction wave recorded in 0.1 M NaPF₆ show that ion migration into the monolayer provides a significant contribution to the cyclic voltammetric response associated with the redox processes. Figure 2c shows a

comparison between cyclic voltammograms of 1^{2+} and 1^{2+} -CB[8] monolayers in PB electrolyte. The first oxidative peak potential ($1^{•+} \rightarrow 1^{2+}$) is slightly more positive (-0.40 V) with CB[8] complexation than without (-0.43 V). On the other hand, the second oxidative peak potential ($1^0 \rightarrow 1^{•+}$) is slightly more negative (-0.68 V) with CB[8] complexation than without (-0.63 V). Differences between the cyclic voltammetry of the 1^{2+} -CB[8] monolayer in NaPF₆ are discussed further in the SI.

Both in PB and NaPF₆ electrolytes, the peak current height linearly increased with the scan rate. The linear relationship between peak current and scan rate for both 1^{2+} and 1^{2+} -CB[8] is consistent with surface immobilization of the redox-active viologen moiety. From integration of the $1^{2+} \rightarrow 1^{•+}$ redox wave in Figure 2a, the coverage of 1^{2+} was estimated to be 5.0×10^{-10} mol/cm². This is consistent with previous reports⁴⁴ and demonstrates that a high coverage self-assembled monolayer of 1^{2+} has been formed on the Au(111) surface. Similar analysis of Figure 2b shows the coverage of 1^{2+} -CB[8] to be 1.5×10^{-10} mol/cm², which is considerably lower than that of the 1^{2+} monolayer due to the large spatial requirement of CB[8].

Compounds 2^{2+} and 3^{2+} are thioethers, in contrast to 1^{2+} , which has thiol end groups. It is not possible to form self-assembled monolayers from thioethers. Thus, we performed aqueous solution electrochemistry for 2^{2+} , 3^{2+} , and their complexes with CB[8] (details of which can be found in the SI). The CVs of 2^{2+} (and also 3^{2+}) before and after CB[8] complexation demonstrated the reduction potential of 2^{2+} (3^{2+}) exhibited little change after CB[8] complexation (Figures S24 and S25).

Single Molecule Conductance. A noncontact STM technique for forming molecular junctions (the so-called $I(s)$ technique) was used to determine the single-molecule conductance of 1^{2+} , 1^{2+} -CB[8], 2^{2+} , 2^{2+} -CB[8], 3^{2+} , and 3^{2+} -CB[8] in aqueous solution. This technique relies on approaching the STM tip to high set-point current values and then recording current (I) as a function of tip retraction distance (s) as the tip is rapidly retracted. Since a large proportion of such $I(s)$ retraction events do not lead to capture of molecules in the junction, those specific to molecular junction formation are recognized by characteristic current plateaus and recorded. At least 500 such molecular junction formation scans were recorded for each viologen compound and their CB[8] complex (see Figure S27 for examples of molecular junction formation $I(s)$ scans). For 1^{2+} , a single molecular conductance in water of 0.49 nS was determined (Figure 3 a, middle). This value closely agrees with values reported in the literature.⁵ Figure 3a, right, shows a two-dimensional (2-D) histogram representation of the data, with conductance on the ordinate, distance on the abscissa (corrected for the initial tip-substrate distance at the start of the $I(s)$ scan), and the color representing the point density ranging from blue (very low) to green to red (high point count). High point counts are seen at conductance values corresponding to the peak in the 1D histogram, and also a high count tail is seen at the base of the plot which corresponds to low conductance values at the break-off region, with the junction conductance dropping toward the noise floor after the molecular bridge cleaves. According to the 2D histogram (Figure 3, b, right), the break-off distance of 1^{2+} -CB[8] is 2.1 nm. This is close to the length of a 1^{2+} molecule, given that molecular modeling of the free molecule produces a distance

between the two sulfur atoms of 2.4 nm for trans-oriented alkyl chains. This implies that polymethylene chains of 1^{2+} are extended out and away from the CB[8] cavity in the 1^{2+} -CB[8] single molecule conductance measurement as schematically depicted in Figure 3b, left.

The peak conductance value for the 1^{2+} -CB[8] complex is 1.67 nS (Figure 3b, middle and right). This clearly demonstrates that formation of the host-guest complex increases the conductance of 1^{2+} more than 3-fold. It has been reported that the conductance of 1^{2+} increased from 0.5 to 2.8 nS when 1^{2+} was electrochemically reduced from the dication to the radical cation states.⁵ For 2^{2+} , the conductance was found to be 0.84 nS in water, which increased to 1.65 nS upon complexation with CB[8] (Figure 3d, middle and right). The conductance of 3^{2+} was 1.57 nS in water (Figure 3e, middle and right), and the conductance of the 3^{2+} -CB[8] complex was 4.2 nS (Figure 3f, middle and right). The small additional peaks for 3.2 nS in Figure 3d and 8.0 nS in Figure 3f at roughly twice the conductance of the principle histogram peak (1.65 and 4.2 nS) are most probably attributed to “double junctions”⁸⁴ (two molecules simultaneously attached between tip and surface).

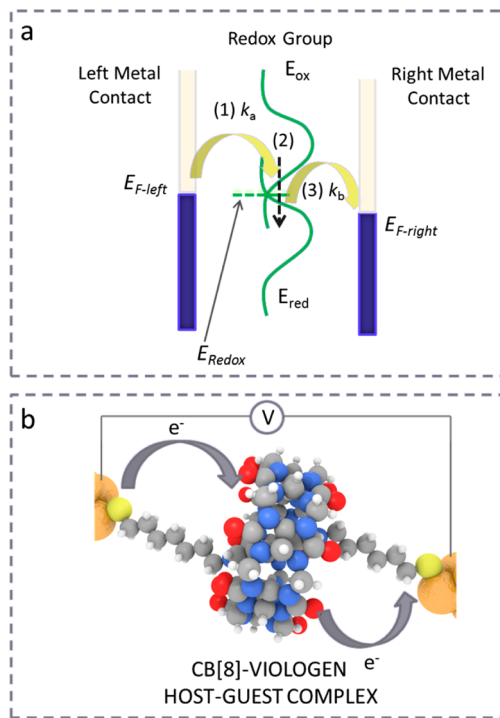
DISCUSSION

The conductance changes observed for the viologen wires 1^{2+} , 2^{2+} and 3^{2+} upon complexation with CB[8] are now discussed in terms of possible mechanisms for electron transfer across the molecular junction, also by taking into account electronic and structural characterization data. It is first noted that in each case the characterization data, and in particular the mass spectroscopy and ¹H NMR in solution, support a 1:1 stoichiometry between host and guest. Only in the case of 2^{2+} associating with CB[8] there is a small signal that corresponds to the binding of two CB[8] molecules by a single 2^{2+} seen in the HRMS (ESI⁺, Q-TOF) spectra. The NMR spectra for 1^{2+} and 3^{2+} threaded within the CB[8] host shows that the viologen core is enclosed symmetrically within the CB[8] host. The additional complexity of the ¹H NMR spectra reported above for 2^{2+} -CB[8] is rationalized in terms of an asymmetrical placement of the 2^{2+} guest with respect to the host cavity. Compound 1^{2+} exhibits a relatively straightforward UV/vis spectrum with an intense absorbance at ~ 260 nm, which is assigned to a $\pi \rightarrow \pi^*$ transition of the bipyridinium core. Notably, this transition hardly changes in energy upon complexation with CB[8], although its absorbance does decrease slightly. Alongside this characteristic absorption band, 2^{2+} and 3^{2+} also exhibit a lower energy transition which is attributed to an intramolecular charge transfer involving the bipyridinium core and appended benzyl (2^{2+}) or phenyl (3^{2+}) rings. The appreciable solvatochromism of this transition supports this assignment. Electrochemical data for self-assembled monolayers of 1^{2+} on Au(111) shows the formation of a high coverage phase. This coverage is greatly reduced for 1^{2+} -CB[8] monolayers due to the large spatial requirement of CB[8]. The reduction potential for 1^{2+} only shows a very small change when complexed with the CB[8] host.

Electron transfer across molecular junctions is generally considered to occur through either tunneling (or superexchange) mechanisms or incoherent hopping type mechanisms. Electron transfer through Au| 1^{2+} |Au single molecule electrical junctions has been studied in detail using STM under electrochemical potential control. The single molecule conductance increased about 6-fold (from 0.5 to 2.8 nS)

following electrochemical reduction of the viologen dication to its cation radical. This electrochemical gating effect has been interpreted within the framework of the two-step hopping model of Kuznetsov and Ulstrup (Scheme 2, a).⁴⁵ In this

Scheme 2. (a) Illustration of the Two-Step Adiabatic Kuznetsov–Ulstrup Model Used, Showing the Two Gold Electrodes (“Left” and “Right”) and the Redox States of the Molecular Bridge in between; (b) Scheme of Viologen–CB[8] Molecular Junction



model, an electron is transferred (hops) from one gold electrode leading to reduction (step 1) and then partial relaxation (step 2) of the system. A second, subsequent electron-transfer step from the now reduced viologen group to the other gold electrode (step 3) of the junction completes the electron-transfer process. Due to the electrochemical nature of these electron-transfer processes, the redox center is subject to reorganization through environmental and internal fluctuations prior to the electron transfer steps, which then proceed through Franck–Condon-type transitions.

In light of the 6-fold increase upon electrochemically reducing the viologen dication to its cation radical, the conductance increase when free I^{2+} ($Au|I^{2+}|Au$ 0.5 nS) is complexed to form $Au|I^{2+}-CB[8]|Au$ junctions (1.67 nS) is substantial. UV/vis spectroscopy shows that the optical band gaps of I^{2+} and $I^{2+}-CB[8]$ are practically identical. This would imply that the conductance change cannot be attributed to changes in the HOMO/LUMO gap. The lack of change in the optical band gap also implies that the bipyridinium moiety does not change substantially in terms of conjugation or configuration when it is threaded into the CB[8] host. The electrochemical potential for reduction of the bipyridinium moiety for monolayers of I^{2+} and $I^{2+}-CB[8]$ on Au(111) are also very similar. This would also imply minor differences in alignment between the contact Fermi energies and the frontier LUMO orbitals in the two-terminal molecular junctions. This invariance in the orbital alignment and band gap within this

system would go against a simple tunneling (or super-exchange)-type mechanism of electron transfer, and as such, the focus in the following text is on incoherent hopping transport and the Kuznetsov–Ulstrup model. Likewise, there are only small changes in the optical bandgap of the redox active bipyridinium core in both 2^{2+} and 3^{2+} (see the SI). In the case of 2^{2+} , the intense absorbance at 260 nm, which is assigned to a $\pi \rightarrow \pi^*$ transition of the bipyridinium core, does not change much; for 2^{2+} , it shifts from 265 to 270 nm (Figure S15a), while for 3^{2+} , it shifts from 264 to 279 nm. The additional absorbance band at higher wavelength observed for 2^{2+} and 3^{2+} is attributed to charge transfer between the electron-rich thioanisole and the electron-deficient 2,2'-bipyridine core and therefore less indicative of electron transport via the redox active core (as described here by the Kuznetsov–Ulstrup model). In addition, the electrochemical reduction potential changes little for 2^{2+} and 3^{2+} before and after CB[8] complexation (Figure S24 and S25). This would also imply minor differences in alignment between the Fermi energies and the frontier LUMO orbitals in the two-terminal molecular junctions.

The two-step hopping-type model of Kuznetsov and Ulstrup⁴⁵ (Scheme 2 a) centers around derivation of rate constants for electron transfer onto the bridge, partial vibrational relaxation of the redox center, and then subsequent electron transfer to the other electrode also modeled by electron-transfer rate equations. The rate constants for electron transfer in the adiabatic limit onto the bridge (k_a for step 1, in Scheme 2a) and sequential electron transfer off the bridge (k_b for step 3) have the following form:⁴⁶

$$k_a \approx \frac{\omega_{\text{eff}}}{2\pi} \exp\left[-\frac{[\lambda - e\eta - \gamma eV_{\text{bias}}]^2}{4\lambda k_B T}\right]$$

$$k_b \approx \frac{\omega_{\text{eff}}}{2\pi} \exp\left[-\frac{[\lambda + e\eta - (1 - \gamma)eV_{\text{bias}}]^2}{4\lambda k_B T}\right] \quad (1)$$

Here, λ is the reorganization energy, e is the charge on an electron, V_{bias} is the bias voltage, η is the overpotential, k_B is Boltzmann's constant, T is the temperature, γ is the fraction of the bias voltage at the site of the redox center, ξ is the fraction of the electrochemical potential experienced at the redox site, and ω_{eff} is a characteristic nuclear vibrational frequency. In this two-step process, the steady-state current across the junction is given, in the limit of strong electronic interactions between the molecular redox group and the electrodes, by⁴⁶

$$i_{\text{tunn}}^{\text{strong}} = 2en_{\text{el}} \frac{k_a k_b}{k_a + k_b} \quad (2)$$

Here, n_{el} is the number of electrons transferred through the molecular junction, while the redox level relaxes after the first electron-transfer step of the sequential electron transfer across the electrical junction.⁴⁶ The reorganization energy, λ , has two contributions, one from the outer sphere and one from the inner sphere. In the case of the viologen bridge system here, the spectroscopic and electrochemical data indicate that the bipyridinium center and its reduction are very similar in the absence and presence of the CB[8] host. The larger size of the cavity compared to the bipyridinium moiety would lead one to expect that this moiety is free to rotate in the cavity. Simulated UV spectra shown in the SI (Figure S28) demonstrate a significant red shift in the spectral absorbance of I^{2+} when the

dihedral angle between the two rings in the bipyridinium moiety changes from twisted to flat. Since the experimentally recorded UV/vis spectra of 1^{2+} demonstrate great similarity between the optical band gap for the bipyridinium moiety with and without CB[8], this implies no significant change in electronic structure of the bipyridinium core upon threading into CB[8]. Likewise, the $\pi \rightarrow \pi^*$ transition of the bipyridinium core of 2^{2+} and 3^{2+} shows only minor changes upon CB[8] complexation (see spectra in the SI).

Taking these observations into account, it seems reasonable to assume that the inner sphere organization energies for the bipyridinium center are similar in the absence and presence of the CB[8] host. Attention is therefore directed toward outer-sphere contributions and the medium surrounding the viologen moiety. The environment has been shown to have a strong bearing on the conductance of single molecular wires, and this has been generally considered within phase-coherent models for charge transport involving DFT computations.^{25,47,48} Within phase-incoherent hopping and Marcus theory type models, changes in the environment would be accompanied by changes in the medium dielectric properties, and this in turn would be anticipated to impact the outer sphere reorganization energies since these are controlled by the dielectric displacement. This can be seen by taking the simplest case of a spherical ion placed in front of a metal electrode surface. An expression for the outer reorganization energy, taking into account the full image charge interaction, is given by the following equation calculated using a macroscopic electrostatic model (*i.e.*, not taking into account molecular structure and dynamics of the dielectric medium)⁴⁹

$$\lambda_{\text{out}} = \frac{1}{2\epsilon_0} \left(\frac{1}{\epsilon_{\infty}} - \frac{1}{\epsilon_s} \right) \left(\frac{1}{a} - \frac{1}{2d} \right) \quad (3)$$

where ϵ_0 is the permittivity of free space, ϵ_{∞} is the optical value of the dielectric constant, and ϵ_s is the static value of the dielectric constant. The radius of the ion is a and d is the distance from the electrode surface.⁴⁹ For constant electron-transfer reaction parameters (a and d in eq 3) changes in λ_{out} can be clearly induced by changes in the Pekar factor, $c_0 = \left(\frac{1}{\epsilon_{\infty}} - \frac{1}{\epsilon_s} \right)$. Generally, this Pekar factor would be expected to only vary slightly with changes in ϵ_s for high static dielectric media like water. However, large changes in this factor have been predicted for dramatic medium changes. For instance, as described by Krishtalik,⁵⁰ changing from water ($c_0 \approx 0.54$) to a nominal protein environment with ϵ_s taken as equal to 4, gives $c_0 \approx 0.15$ (*i.e.*, a factor of 3 change in the Pekar factor). Krishtalik describes how the low static dielectric permittivity of proteins (compared to water) gives rise to the low reorganization energies for electron transfer within them.⁵⁰ In a similar manner, we hypothesize here that a low static dielectric permittivity within the CB[8] could explain the higher conductance for viologens introduced into this host. Simulations by Biedermann *et al.* show that the CB[8] cavity incorporating the viologen guest contains also a residual amount of water molecules whose conformational space and hydrogen bonding ability is restricted by the cavity.³¹ They describe these water molecules which are situated in the hydrophobic cavity as “high energy”.³¹ This placement of the water at the hydrophobic cavity surface and the restricted hydrogen bonding ability would be expected to impact the

water environment and also consequently the medium dielectric properties.

The factor by which the conductance increases upon threading the viologen into the CB[8] host is largest for 1^{2+} (a factor of 3.4). The corresponding factor for 2^{2+} is 2.0, while it is 2.7 for 3^{2+} . A possible explanation for this difference is the CB[8] position on the viologen derivative. According to the results of ^1H NMR and $^1\text{H}, ^1\text{H}$ -COSY, the positively charged bipyridinium moiety of 1^{2+} and 3^{2+} are positioned inside the CB[8] cavity. However, for 2^{2+} , one phenyl group and half of the bipyridinium moiety is positioned in the CB[8] cavity. This reduced encapsulation within the CB[8] cavity could explain the lower factor by which the conductance increases upon host:guest complexation for 2^{2+} .

CONCLUSIONS

In conclusion, we have investigated the molecule conductance values of viologen–CB[8] host–guest complexes. The conductance of viologen derivatives increases upon encapsulation within the hydrophobic CB[8] cavity, which is interpreted as arising from a reduced outer sphere reorganization energy within the framework of a Marcus-type model for electron transfer. These findings show that the local microenvironment within a supramolecular complex encapsulating the molecular wire has a large impact on the molecule conductance, providing a solid theoretical basis for designing supramolecular electronic devices.

METHODS

Synthesis of 2^{2+} and 3^{2+} . The synthesis of compound 2^{2+} and 3^{2+} can be found in the SI.

Solution Preparation of Viologen–CB[8] Complexes. The 1^{2+} –CB[8] aqueous solution (1 mM) was prepared by adding CB[8] powder into a 1 mM solution of 1^{2+} under sonication until all powder dissolved, and then this solution was allowed to stand overnight. 2^{2+} –CB[8] (1 mM) and 3^{2+} –CB[8] (0.5 mM) solutions were prepared in a similar manner. For the STM experiments, the 100 μM 1^{2+} , 1^{2+} –CB[8], 2^{2+} , 2^{2+} –CB[8], 3^{2+} , and 3^{2+} –CB[8] aqueous solutions were prepared by dilution of 1 or 0.5 mM sample solutions. Phosphate buffer (0.1 M, pH 6.98) and NaPF_6 (0.1 M, pH 2.48) was used as supporting electrolyte for electrochemistry.

UV/vis, ^1H NMR, $^1\text{H}, ^1\text{H}$ -COSY Spectra Measurement. For the study of host–guest complexation of CB[8] and guests, 100 μM CB[8], 1 mM 1^{2+} , 1^{2+} –CB[8], 2^{2+} , 2^{2+} –CB[8], 0.5 mM 3^{2+} , and 3^{2+} –CB[8] solutions were prepared in D_2O . NMR spectra were acquired on a Bruker 500 MHz Avance III spectrometer at ambient temperature. ^1H NMR spectra for all compounds were acquired using solvents suppression via either presaturation or a WATERGATE scheme (water suppression by gradient tailored excitation), while $^1\text{H}, ^1\text{H}$ -COSY included a presaturation sequence. In addition, 40 μM 1^{2+} , 32.5 μM 2^{2+} , 100 μM 3^{2+} , and their CB[8] complex solutions containing different concentrations of CB[8] were prepared for obtaining absorption spectra on a UV-2550 from SHIMADZU at room temperature. Mass spectra were recorded using a Micromass LCT (ESI⁺) or Agilent 6530 LC/MS (ESI⁺, Q-TOF) mass spectrometers.

Electrochemical Experiments. All cyclic voltammetry measurements were performed on EcoChemie Autolab potentiostats, either the PGSTAT 20 or PGSTAT 30 model with the corresponding Autolab GPES software. A three-electrode setup was used, with a Au(111) working electrode (WE), Pt wire mesh counter-electrode (CE), and SCE as the reference electrode. The electrode surface area of the Au(111) WE was the measured geometric area in contact with the electrolyte. The glass electrochemical cell was cleaned in a 10% HNO_3 (aq) solution prior to use and rinsed several times in Milli-Q

water. The CE and WE were flame annealed prior to use. The cell was dried in an oven at 150 °C before use.

For electrochemistry of the 1^{2+} monolayers, the Au (111) bead electrode was immersed in 1 mM 1^{2+} ethanol solution for 18 min at 70 °C with N_2 protection and then rinsed with ethanol and water before being inserted into the electrochemistry cell containing degassed 0.1 M phosphate buffer or 0.1 M $NaPF_6$ electrolyte. For electrochemistry of the 1^{2+} -CB[8] monolayer, the aforementioned 1^{2+} monolayer modified Au(111) bead electrode was immersed into the saturated CB[8] solution for 2 h at 40 °C under an inert N_2 atmosphere and then rinsed with water before being inserted into the electrochemical cell containing 0.1 M phosphate buffer or 0.1 M $NaPF_6$ with N_2 degassing.

Single-Molecule Conductance Measurements. All of the single-molecule experiments were performed using an Agilent 5500 STM controller in conjunction with the Agilent Picoscan 5.3.3 software. Au STM tips were prepared using 0.25 mm Au wire (99.99%, Goodfellow), which were electrochemically etched in a 1:1 solution of HCl and ethanol at approximately +7.0 V. The Au tips were then coated with a layer of Apiezon wax, ensuring that only the very end of the tip was exposed. Commercial gold-on-glass substrates (Arrandee) were flame annealed for approximately 5 min prior to use, but care was taken to avoid overheating. For the STM measurements, all adlayers were formed on the gold-on-glass substrate by immersing the substrate in the 100 μ M sample solution for 1 min. The gold electrode was then rinsed with ethanol, water, and acetone and blown dry using N_2 . After the gold sample was installed into the STM cell, 100 μ L of water was added to the solution cell followed by about 10 μ L of the 50 μ M complex solution and 10 μ L of 50 μ M CB[8]. STM measurements were then made.

The STM $I(s)$ technique was employed for single-molecule conductance determination with a set-point current (I_0) of 40 nA and a sample bias voltage (V_{bias}) of +0.6 V. To record current (I) versus retraction distance (s) curves, the tip was withdrawn from the set-point distance by 4 nm with a retraction duration of 0.1 s. Those scans which showed molecular junction formation were plotted into a histogram, which was used to find the molecular conductance.

ASSOCIATED CONTENT

Supporting Information

The Supporting Information is available free of charge on the ACS Publications website at DOI: 10.1021/acsnano.6b00786. All the data is available on the data catalog in Liverpool <http://datacat.liverpool.ac.uk/86/>.

Experimental details, Figures S1–S28, and Tables S1–S5 (PDF)

Crystallographic data for 3^{2+} (CIF)

AUTHOR INFORMATION

Corresponding Authors

*E-mail: nichols@liv.ac.uk.

*E-mail: lniu@ciac.ac.cn.

Notes

The authors declare no competing financial interest.

ACKNOWLEDGMENTS

R.J.N. and S.J.H. thank EPSRC for funding (grant EP/H035184/1 and EP/K007785/1). This work was also supported by the grant “Electronanomat” (Molecular Scale Electrochemistry and Nontraditional Electrochemical Materials Science, project reference 318990) from the European Union (Seventh Framework Programme, Marie Curie Programme), NSFC, China (No.21225524, 21375124, 21575136, 21505127) and Funds for the Construction of Taishan Scholars (No.ts201511058). W.Z. acknowledges a joint PhD studentship

from China Scholarship Council. A.B. and R.J.D. also gratefully acknowledge the EPSRC (EP/K007785/1; EP/K007548/1) for funding this work and Dmitry Yufit for obtaining the crystal structure of 3^{2+} . P.J.L. gratefully acknowledges support from the ARC (DP140100855) and the award of a Future Fellowship (FT120100073). B.L. gratefully acknowledges support from the EPSRC for funding (grant EP/K014773/1).

REFERENCES

- (1) Reed, M. A.; Zhou, C.; Muller, C. J.; Burgin, T. P.; Tour, J. M. Conductance of a Molecular Junction. *Science* **1997**, *278*, 252–254.
- (2) Kergueris, C.; Bourgoignie, J. P.; Palacin, S.; Esteve, D.; Urbina, C.; Magoga, M.; Joachim, C. Electron Transport through a Metal-Molecule-Metal Junction. *Phys. Rev. B: Condens. Matter Mater. Phys.* **1999**, *59*, 12505–12513.
- (3) Weber, H. B.; Reichert, J.; Weigend, F.; Ochs, R.; Beckmann, D.; Mayor, M.; Ahlrichs, R.; von Lohneysen, H. Electronic Transport through Single Conjugated Molecules. *Chem. Phys.* **2002**, *281*, 113–125.
- (4) Xu, B. Q.; Tao, N. J. Measurement of Single-Molecule Resistance by Repeated Formation of Molecular Junctions. *Science* **2003**, *301*, 1221–1223.
- (5) Haiss, W.; van Zalinge, H.; Higgins, S. J.; Bethell, D.; Hobenreich, H.; Schiffrin, D. J.; Nichols, R. J. Redox State Dependence of Single Molecule Conductivity. *J. Am. Chem. Soc.* **2003**, *125*, 15294–15295.
- (6) Haiss, W.; Nichols, R. J.; van Zalinge, H.; Higgins, S. J.; Bethell, D.; Schiffrin, D. J. Measurement of Single Molecule Conductivity Using the Spontaneous Formation of Molecular Wires. *Phys. Chem. Chem. Phys.* **2004**, *6*, 4330–4337.
- (7) Cui, X. D.; Primak, A.; Zarate, X.; Tomfohr, J.; Sankey, O. F.; Moore, A. L.; Moore, T. A.; Gust, D.; Harris, G.; Lindsay, S. M. Reproducible Measurement of Single-Molecule Conductivity. *Science* **2001**, *294*, 571–574.
- (8) Marqués-González, S.; Low, P. J. Molecular Electronics: History and Fundamentals. *Aust. J. Chem.* **2016**, *69*, 244–253.
- (9) Venkataraman, L.; Klare, J. E.; Nuckolls, C.; Hybertsen, M. S.; Steigerwald, M. L. Dependence of Single-Molecule Junction Conductance on Molecular Conformation. *Nature* **2006**, *442*, 904–907.
- (10) Sedghi, G.; Garcia-Suarez, V. M.; Esdaile, L. J.; Anderson, H. L.; Lambert, C. J.; Martin, S.; Bethell, D.; Higgins, S. J.; Elliott, M.; Bennett, N.; et al. Long-Range Electron Tunneling in Oligo-Porphyrin Molecular Wires. *Nat. Nanotechnol.* **2011**, *6*, 517–523.
- (11) Kolivoska, V.; Valasek, M.; Gal, M.; Sokolova, R.; Bulickova, J.; Pospisil, L.; Meszaros, G.; Hromadova, M. Single-Molecule Conductance in a Series of Extended Viologen Molecules. *J. Phys. Chem. Lett.* **2013**, *4*, 589–595.
- (12) Wang, C.; Batsanov, A. S.; Bryce, M. R.; Martin, S.; Nichols, R. J.; Higgins, S. J.; Garcia-Suarez, V. M.; Lambert, C. J. Oligoynone Single Molecule Wires. *J. Am. Chem. Soc.* **2009**, *131*, 15647–15654.
- (13) Moreno-Garcia, P.; Gulcur, M.; Manrique, D. Z.; Pope, T.; Hong, W.; Kaliginedi, V.; Huang, C.; Batsanov, A. S.; Bryce, M. R.; Lambert, C.; et al. Single-Molecule Conductance of Functionalized Oligoynes: Length Dependence and Junction Evolution. *J. Am. Chem. Soc.* **2013**, *135*, 12228–12240.
- (14) van der Molen, S. J.; Liljeroth, P. Charge Transport through Molecular Switches. *J. Phys.: Condens. Matter* **2010**, *22*, 133001–1–30.
- (15) Nichols, R. J.; Higgins, S. J. In *Electrocatalysis: Theoretical Foundations and Model Experiments*; Alkire, R. C., Kolb, D. M., Lipkowsky, J., Eds.; John Wiley and Sons, 2013; Chapter 3.
- (16) Coskun, A.; Spruell, J. M.; Barin, G.; Dichtel, W. R.; Flood, A. H.; Botros, Y. Y.; Stoddart, J. F. High Hopes: Can Molecular Electronics Realise Its Potential? *Chem. Soc. Rev.* **2012**, *41*, 4827–4859.
- (17) Wu, S. M.; Gonzalez, M. T.; Huber, R.; Grunder, S.; Mayor, M.; Schonenberger, C.; Calame, M. Molecular Junctions Based on Aromatic Coupling. *Nat. Nanotechnol.* **2008**, *3*, 569–574.

- (18) Martin, S.; Grace, I.; Bryce, M. R.; Wang, C.; Jitchati, R.; Batsanov, A. S.; Higgins, S. J.; Lambert, C. J.; Nichols, R. J. Identifying Diversity in Nanoscale Electrical Break Junctions. *J. Am. Chem. Soc.* **2010**, *132*, 9157–9164.
- (19) Nishino, T.; Hayashi, N.; Bui, P. T. Direct Measurement of Electron Transfer through a Hydrogen Bond between Single Molecules. *J. Am. Chem. Soc.* **2013**, *135*, 4592–4595.
- (20) Bui, P. T.; Nishino, T.; Yamamoto, Y.; Shiigi, H. Quantitative Exploration of Electron Transfer in a Single Noncovalent Supramolecular Assembly. *J. Am. Chem. Soc.* **2013**, *135*, 5238–5241.
- (21) Vezzoli, A.; Grace, I.; Brooke, C.; Wang, K.; Lambert, C. J.; Xu, B.; Nichols, R. J.; Higgins, S. J. Gating of Single Molecule Junction Conductance by Charge Transfer Complex Formation. *Nanoscale* **2015**, *7*, 18949–18955.
- (22) Garcia, R.; Angeles Herranz, M.; Leary, E.; Gonzalez, M. T.; Rubio Bollinger, G.; Buerkle, M.; Zotti, L. A.; Asai, Y.; Pauly, F.; Carlos Cuevas, J.; et al. Single-Molecule Conductance of a Chemically Modified, Pi-extended Tetrathiafulvalene and Its Charge-Transfer Complex with F(4)TCNQ. *Beilstein J. Org. Chem.* **2015**, *11*, 1068–1078.
- (23) Huang, S.; He, J.; Chang, S.; Zhang, P.; Liang, F.; Li, S.; Tuchband, M.; Fuhrmann, A.; Ros, R.; Lindsay, S. Identifying Single Bases in a DNA Oligomer with Electron Tunneling. *Nat. Nanotechnol.* **2010**, *5*, 868–873.
- (24) Kiguchi, M.; Nakashima, S.; Tada, T.; Watanabe, S.; Tsuda, S.; Tsuji, Y.; Terao, J. Single-Molecule Conductance of π -Conjugated Rotaxane: New Method for Measuring Stipulated Electric Conductance of π -Conjugated Molecular Wire Using STM Break Junction. *Small* **2012**, *8*, 726–730.
- (25) Leary, E.; Hobenreich, H.; Higgins, S. J.; van Zalinge, H.; Haiss, W.; Nichols, R. J.; Finch, C. M.; Grace, I.; Lambert, C. J.; McGrath, R.; et al. Single-Molecule Solvation-Shell Sensing. *Phys. Rev. Lett.* **2009**, *102*, No. 086801-1-4.
- (26) Lee, J. W.; Samal, S.; Selvapalam, N.; Kim, H. J.; Kim, K. Cucurbituril Homologues and Derivatives: New Opportunities in Supramolecular Chemistry. *Acc. Chem. Res.* **2003**, *36*, 621–630.
- (27) Kim, H. J.; Heo, J.; Jeon, W. S.; Lee, E.; Kim, J.; Sakamoto, S.; Yamaguchi, K.; Kim, K. Selective Inclusion of a Hetero-Guest Pair in a Molecular Host: Formation of Stable Charge-Transfer Complexes in Cucurbit[8]uril. *Angew. Chem., Int. Ed.* **2001**, *40*, 1526–1529.
- (28) Bush, M. E.; Bouley, N. D.; Urbach, A. R. Charge-Mediated Recognition of N-Terminal Tryptophan in Aqueous Solution by a Synthetic Host. *J. Am. Chem. Soc.* **2005**, *127*, 14511–14517.
- (29) Jeon, W. S.; Kim, E.; Ko, Y. H.; Hwang, I. H.; Lee, J. W.; Kim, S. Y.; Kim, H. J.; Kim, K. Molecular loop lock: A Redox-Driven Molecular Machine Based on a Host-Stabilized Charge-Transfer Complex. *Angew. Chem., Int. Ed.* **2005**, *44*, 87–91.
- (30) Biedermann, F.; Scherman, O. A. Cucurbit[8]uril Mediated Donor-Acceptor Ternary Complexes: A Model System for Studying Charge-Transfer Interactions. *J. Phys. Chem. B* **2012**, *116*, 2842–2849.
- (31) Biedermann, F.; Vendruscolo, M.; Scherman, O. A.; De Simone, A.; Nau, W. M. Cucurbit[8]uril and Blue-Box: High-Energy Water Release Overwhelms Electrostatic Interactions. *J. Am. Chem. Soc.* **2013**, *135*, 14879–14888.
- (32) Jiang, S.; Yang, X.; Yang, C.; Tong, M.; Zou, D.; Wu, Y. Guest-Size Determining the Selective Binding Modes of Cucurbit[8]uril, Electron-Rich Guests and N-Alkyl-N'-Methyl-4,4'-Bipyridinium. *Tetrahedron Lett.* **2013**, *54*, 1638–1644.
- (33) Hu, C.; Lan, Y.; Tian, F.; West, K. R.; Scherman, O. A. Facile Method for Preparing Surface-Mounted Cucurbit[8]uril-Based Rotaxanes. *Langmuir* **2014**, *30*, 10926–10932.
- (34) Jeon, W. S.; Kim, H. J.; Lee, C.; Kim, K. Control of the Stoichiometry in Host-Guest Complexation by Redox Chemistry of Guests: Inclusion of Methylviologen in Cucurbit[8]uril. *Chem. Commun.* **2002**, 1828–1829.
- (35) Kim, H. J.; Jeon, W. S.; Ko, Y. H.; Kim, K. Inclusion of Methylviologen in Cucurbit[7]uril. *Proc. Natl. Acad. Sci. U. S. A.* **2002**, *99*, 5007–5011.
- (36) Ong, W.; Gomez-Kaifer, M.; Kaifer, A. E. Cucurbit[7]uril: A Very Effective Host for Viologens and Their Cation Radicals. *Org. Lett.* **2002**, *4*, 1791–1794.
- (37) Moon, K.; Kaifer, A. E. Modes of Binding Interaction between Viologen Guests and the Cucurbit[7]uril Host. *Org. Lett.* **2004**, *6*, 185–188.
- (38) Ong, W.; Kaifer, A. E. Salt Effects on the Apparent Stability of the Cucurbit[7]uril-Methyl Viologen Inclusion Complex. *J. Org. Chem.* **2004**, *69*, 1383–1385.
- (39) Xiao, X.; Tao, Z.; Xue, S.-F.; Zhu, Q.-J.; Zhang, J.-X.; Lawrance, G. A.; Raguse, B.; Wei, G. Interaction between Cucurbit[8]uril and Viologen Derivatives. *J. Inclusion Phenom. Mol. Recognit. Chem.* **2008**, *61*, 131–138.
- (40) Haiss, W.; Nichols, R. J.; Higgins, S. J.; Bethell, D.; Hobenreich, H.; Schiffrin, D. J. Wiring Nanoparticles with Redox Molecules. *Faraday Discuss.* **2004**, *125*, 179–194.
- (41) Haiss, W.; van Zalinge, H.; Hobenreich, H.; Bethell, D.; Schiffrin, D. J.; Higgins, S. J.; Nichols, R. J. Molecular Wire Formation from Viologen Assemblies. *Langmuir* **2004**, *20*, 7694–7702.
- (42) Park, Y. S.; Whalley, A. C.; Kamenetska, M.; Steigerwald, M. L.; Hybertsen, M. S.; Nuckolls, C.; Venkataraman, L. Contact Chemistry and Single-Molecule Conductance: A Comparison of Phosphines, Methyl Sulfides, and Amines. *J. Am. Chem. Soc.* **2007**, *129*, 15768–15769.
- (43) Leary, E.; La Rosa, A.; Gonzalez, M. T.; Rubio-Bollinger, G.; Agrait, N.; Martin, N. Incorporating Single Molecules into Electrical Circuits. The Role of the Chemical Anchoring Group. *Chem. Soc. Rev.* **2015**, *44*, 920–942.
- (44) Li, Z.; Han, B.; Meszaros, G.; Pobelov, I.; Wandlowski, T.; Blaszczyk, A.; Mayor, M. Two-Dimensional Assembly and Local Redox-Activity of Molecular Hybrid Structures in an Electrochemical Environment. *Faraday Discuss.* **2006**, *131*, 121–143.
- (45) Zhang, J.; Kuznetsov, A. M.; Medvedev, I. G.; Chi, Q.; Albrecht, T.; Jensen, P. S.; Ulstrup, J. Single-Molecule Electron Transfer in Electrochemical Environments. *Chem. Rev.* **2008**, *108*, 2737–2791.
- (46) Zhang, J.; Albrecht, T.; Chi, Q.; Kuznetsov, A. M.; Ulstrup, J. Charge Transfer And Interfacial Bioelectrochemistry At The Nanoscale And Single-Molecule Levels. In *Bioinorganic Electrochemistry*; Hammerich, O., Ulstrup, J., Eds.; Springer: Dordrecht, 2008; pp 249–302.
- (47) Fatemi, V.; Kamenetska, M.; Neaton, J. B.; Venkataraman, L. Environmental Control of Single-Molecule Junction Transport. *Nano Lett.* **2011**, *11*, 1988–1992.
- (48) Milan, D. C.; Al-Owaedi, O. A.; Oerthel, M.-C.; Marqués-González, S.; Brooke, R. J.; Bryce, M. R.; Cea, P.; Ferrer, J.; Higgins, S. J.; Lambert, C. J. Solvent Dependence of the Single Molecule Conductance of Oligoynes-Based Molecular Wires. *J. Phys. Chem. C* **2015**, DOI: 10.1021/acs.jpcc.5b08877.
- (49) Santos, E.; Schmickler, W. *Interfacial Electrochemistry*; Oxford University Press: Oxford, 1996.
- (50) Krishtalik, L. I. The Medium Reorganization Energy for the Charge Transfer Reactions in Proteins. *Biochim. Biophys. Acta, Bioenerg.* **2011**, *1807*, 1444–1456.